

Learned Contextual LiDAR Informed Visual Search in Unseen Environments

Ryan Gupta¹, Kyle Morgenstein¹, Steven Ortega² and Luis Sentis¹

Abstract—This paper presents LIVES: LiDAR Informed Visual Search, an autonomous planner for unknown environments. We consider the pixel-wise environment perception problem where one is given 2D range data from LiDAR scans and must label points contextually as map or non-map in the surroundings for visual planning. LIVES classifies incoming 2D scans from the wide Field of View (FoV) LiDAR in unseen environments without prior map information. The map-generalizable classifier is trained from expert data collected using a simple cart platform equipped with a map-based classifier in real environments. A visual planner takes contextual data from scans and uses this information to plan viewpoints more likely to yield detection of the search target. While conventional frontier based methods for LiDAR and multi sensor exploration effectively map environments, they are not tailored to search for people indoors, which we investigate in this paper. LIVES is baselined against several existing exploration methods in simulation to verify its performance. Finally, it is validated in real-world experiments with a Spot robot in a 20x30m indoor apartment setting. Videos of experimental validation can be found on our project website at <https://sites.google.com/view/lives-icra-2024/home>.

I. INTRODUCTION

Autonomous planning and real-world execution for active search and exploration are receiving significant attention from the robotics community due to their relevance in several scenarios including inspection, surveillance, and Search and Rescue (SAR) [27]. Autonomous ground robots cannot assume reliable map information a priori during active search missions, for example in a disaster response scenario. This demands environment perception tailored for the task of locating any persons in need quickly. Today's robots are frequently equipped with LiDAR sensors that cast a full view of the surroundings. However, use of these scans is often limited to the task of localization and mapping. This paper addresses the exploitation of wide Field of View (FoV) LiDAR scans for visual planning. We propose to classify LiDAR scan points as map or non-map in the robot's surroundings for improved visual search planning.

Several methods exist for pixel-wise classification of 3D LiDAR scans [22, 23, 34]. However, [15] notes that these methods are limited by the high computational requirements to handle to large input size of 3D cloud data. In contrast, real time projection-based methods aim to detect moving obstacles [13] or objects to be avoided in 3D scans, often for autonomous driving applications [18, 5, 20]. Despite parallel improvements in efficiency of planning algorithms for both

LiDAR and vision sensors [6, 14, 28, 32] it remains an open problem to enhance performance in autonomous planning and execution for the task of visual search. There exists a gap of real-time pixel-wise classification of LiDAR scans for active visual search tasks. This work addresses this limitation with an online 2D pixel-wise LiDAR scan classifier and context informed visual planner. In particular, classified LiDAR scans are used to generate highly informative plans quickly with a multisensor Frontier Exploration [33] based planner.

Active planners in unknown spaces are required to make decisions based on incomplete and noisy information about partial environments. State of the art visual task planners like [6, 32] account for LiDAR scans without considering contextual information. We provide a visual planner with map and non-map data in the surroundings found in wide FoV LiDAR scans. This is accomplished by learning to distinguish points unlikely to be permanent features in unknown environments. The visual planner gives priority to features of interest under the assumption that the search target belongs to the set of non-map points. This information obviates the need to visually inspect parts of the environment that are likely to be permanent. An overview of the proposed method can be found in Fig. 1.

The contributions of this work can be summarized as follows:

- A learning strategy for pixel-wise scan classification as map and non-map in unseen, real-world environments
- A formulation that incorporates classified scan information into a planner for visual search
- Demonstrate reduced mission completion time in the visual search task over existing planners
- Deploy and verify the proposed method on a real robotic system in an unseen indoor environment

Sections II, III and IV describe related works, methods and results including baseline comparisons.

II. RELATED WORKS

A. Lidar Classification

Indoor pointcloud classification is tackled in 3D [30] using the KPConv architecture [29]. This method requires the offline annotation and map building at instantiation, and is used for localization and navigation in later work [31]. Neither work validates on a real robot platform. Ref. [21] presents an in depth comparison and framework for Iterative Closest Point (ICP) methods, similar to that of [30], focused on map building. Finally, [26] present a map-free framework for segmenting 3D pointclouds into ground, edges and planar points, which are used in a feature extraction process for mapping environments. In contrast LIVES recognizes non-map features.

¹Department of Aerospace Engineering and Engineering Mechanics, University of Texas at Austin, Austin, TX 78712 USA
ryan.gupta@utexas.edu

²Department of Mechanical Engineering, University of Texas at Austin, Austin, TX 78712 USA

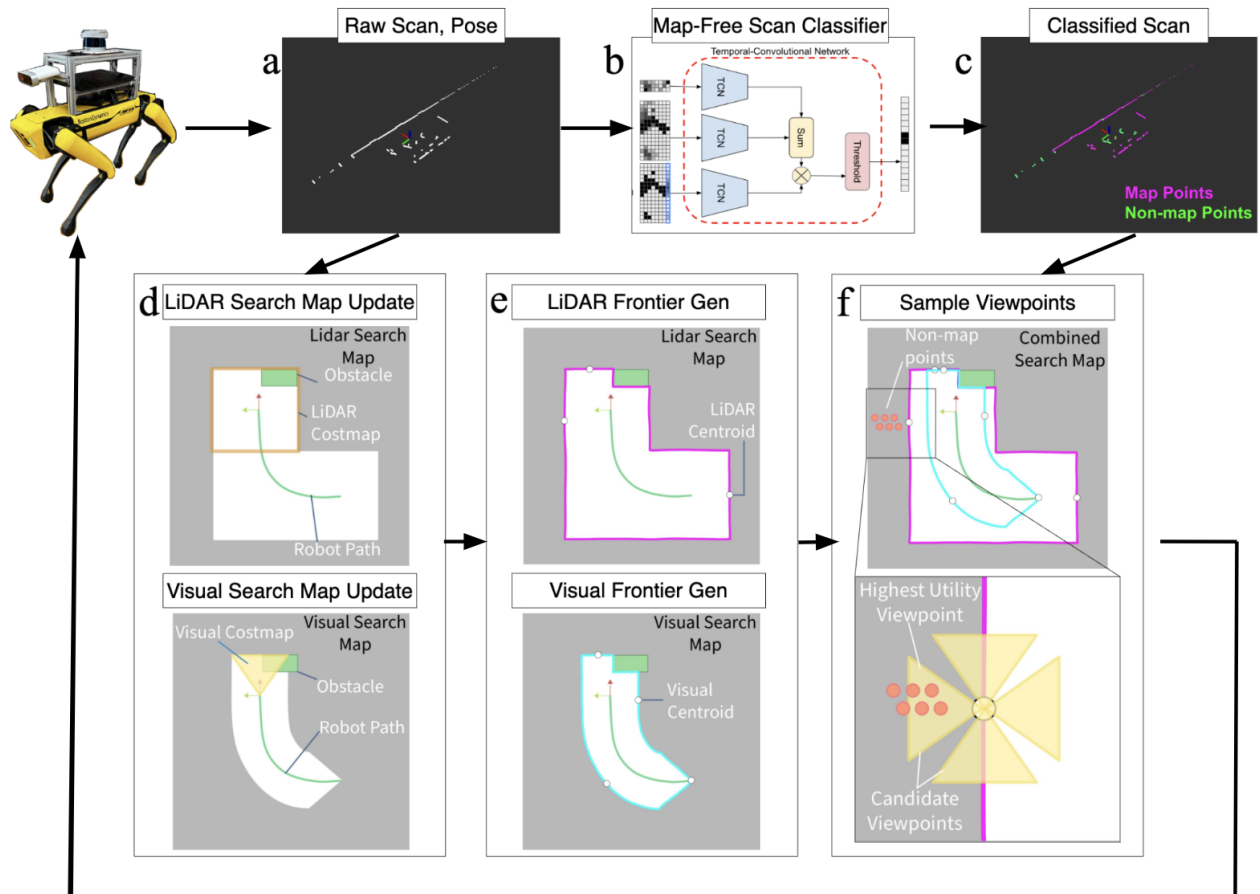


Fig. 1. Overview of LIVES. In (a) raw 2D LiDAR scans, pose information and image data are received from the Spot robot. They are sent through a neural network classifier III-C (b) to label each point as map or non-map (c). Separately, LiDAR scans and pose data are used to maintain the global search maps (d). Global search maps are used to generate frontier points (e), which are used for finding candidate viewpoints. Finally, each frontier point is sampled at four viewpoints (f) and scored III-E2. In this toy example the left viewpoint in (f) will be scored highest and selected as the next waypoint due to the high number of unknown cells and non-map points observed. Finally, the selected viewpoint is sent back to the robot for execution.

B. Next-Best View and Informative Path Planning

Exploration is often solved using next-best viewpoint planners like Frontier Exploration [33, 14]. A common approach uses an active perception formulation to maximize entropy reduction [17, 12]. Ref. [11] learns a policy to generate non-myopic plans online by estimating potential gains of exploring different areas. Ref. [19] similarly learn an information aware policy offline that proposes waypoints for the robot. A local planner then generates dynamically feasible trajectories based on these suggestions. In contrast to the proposed approach, [11, 19] only provide simulation results. Similar to our method, [36] focuses on the problem of visual search. They propose an end-to-end policy that learns to generate discrete actions that lead a robot to a prescribed viewpoint in the given environment, however, the action space is limited to simple discrete actions and they do not leverage LiDAR information. Ref. [35] propose a POMDP planner for generalized local object search in cluttered 3D environments and extend it with a 2D planner for larger areas. In contrast to LIVES, this work is aimed at small areas and small objects, rather than quickly searching buildings for people.

C. World Prediction Based Planning

Often world prediction methods involve learning a model for relevant environments and leveraging their structure for exploring high-value regions first. Ref. [25] use topological features from a database of worlds to inform a frontier-based exploration policy and increase the rate of area explored. Similarly, [28] uses a prediction module that detects semantic objects, classifies frontiers, and predicts information gain beyond those frontiers. A planner uses this to explore rooms fully before continuing global exploration, unlike LIVES that avoids complete exploration to reduce search completion time. Ref. [24] instead consider visual navigation with occupancy anticipation from egocentric RGB-D based visual context. Ref. [10] instead learn to predict locations of exits in building with a convolutional neural network (CNN) using a database of building blueprints. Prediction guide the robot towards likely exit locations.

III. METHODS

The overall scan classifier and planning module are described in Alg. 1. The key components are detailed in this section.

Algorithm 1 Map-Free LiDAR Informed Search()

Input: s_i, x_i

LiDAR Scan, Robot Pose

Output: x_{next}^* (Next viewpoint) $s_i^{\text{class}} = \text{NeuralNetworkClassifier}(s_i)$ $\mathcal{M}_i^{\text{LiDAR}} \leftarrow \text{LiDARMapUpdate}(s_i, x_i, \mathcal{M}_{i-1}^{\text{LiDAR}})$ $\mathcal{M}_i^{\text{Visual}} \leftarrow \text{VisualMapUpdate}(s_i, x_i, \mathcal{M}_{i-1}^{\text{Visual}})$ $\{C^{\text{LiDAR}}\} = \text{GetLiDARFrontiers}(\mathcal{M}_i^{\text{LiDAR}})$ $\{C^{\text{Visual}}\} = \text{GetVisualFrontiers}(\mathcal{M}_i^{\text{Visual}})$ **for** $n \leftarrow 1$ to N **do** ▷ for each frontier c_n in C **for** $j \leftarrow 1$ to 4 **do** ▷ for each viewpoint at c_n $\text{util}_{n,j} = \text{ComputeSampleUtility}(c_n, x_i, s_i^{\text{class}})$ **end for****end for** $x_{\text{next}}^* \leftarrow \arg \max_{n,j} (\text{util}_{n,j})$ **return** x_{next}^*

A. Environment

The environment is described as a discrete set of points \mathcal{E} . This can be split into two subsets $\mathcal{E}^{\text{free}} \subset \mathcal{E}$ and $\mathcal{E}^{\text{occ}} \subset \mathcal{E}$, which represent the free and occupied cells in the environment. Both of these sets are initially unknown to the robot, but are assumed to follow a structure inherent in indoor environments (e.g. hallways, planar walls, open rooms and loops).

B. Ground Truth LiDAR Scan Classification

The search target of interest belongs to $\mathcal{E}^{\text{occ}} \subset \mathcal{E}$. In particular, scan classification attempts to divide \mathcal{E}^{occ} into two subsets, namely $\mathcal{E}^{\text{non-map}}$ and \mathcal{E}^{map} . In this work, \mathcal{E}^{map} are points in the environment that are deemed to be Long-Term Features (LTFs) during classification, while $\mathcal{E}^{\text{non-map}}$ are points that are either Short-Term Features (STFs) or Dynamic Features (DFs) [9]. LTFs represent the static map obstacles, STFs represent static un-mapped obstacles and DFs represent moving points. Given map information, scan points can be classified into these three categories as follows.

Let x_i denote the pose of the robot, and s_i denote observation at time step t_i . Each observation s_i consists of n_i 2D points, $s_i = \{p_i^j\}_{j=1:n_i}$. Observations are transformed from robot local frame into the global frame using an affine transformation $T_i \in SE(3)$. Finally, let map \mathcal{M} be represented as a set of lines $\{l_i\}_{1:n}$.

1) *LTF*: First, an analytic ray cast is performed [8] to determine expected laserscan based on map \mathcal{M} and current robot position x_i . Given observations, the probability that points correspond to one of the lines of that static map can be written

$$P(p_i^j | x_i, \mathcal{M}) = \exp\left(-\frac{\text{dist}(T_i p_i^j, l_j)^2}{\Sigma_s}\right) \quad (1)$$

where Σ_s is the scalar variance of observations, which comes from sensor accuracy. If Eq. 1 is greater than a threshold, point p_i^j is classified as a LTF.

2) *STF*: Remaining points will be classified as STF or DF. Observations at current time i , p_i^j , are compared with prior observations at time k , p_k^l to determine correspondence between points in subsequent observations. The likelihood of

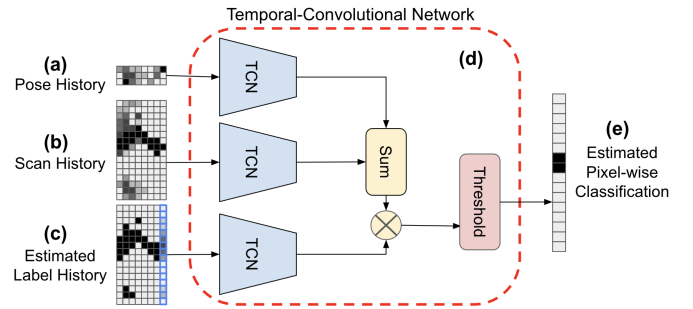


Fig. 2. Pixel-wise LiDAR scan classification model architecture. k is the length of the history buffer. (a) $[3, k]$ pose history matrix containing $[x, y, \theta]$. (b) $[n_i, k]$ LiDAR range history matrix. (c) $[n_i, k - 1] \cup [n_i, 1]$ estimated label history matrix concatenated with its pixel-wise exponential weighted average. (d) The model consists of three temporal-convolutional encoders (TCN), one for each input. The encoded poses, scans, and labels are combined to produce a pixel-wise classification of the LiDAR scan. In (e) a threshold is applied to the raw logits such that each pixel is classified as either a map point or a non-map point.

the remaining points corresponding to the same point as in a previous laserscan is computed as

$$P(p_i^j, p_k^l | x_i, x_k) = \exp\left(-\frac{\|T_i p_i^j - T_k p_k^l\|^2}{\Sigma_s}\right) \quad (2)$$

where p_k^l is the nearest point from p_i^j among points which does not belong to LTF at other timesteps, defined as

$$p_k^l = \arg \min \|T_i p_i^j - T_k p_k^l\| \quad (3)$$

When Eq. 2 is greater than some threshold, point p_i^j is classified as an STF. Remaining points in p_i^j are classified as DFs. The result is classified scan s_i^{class} . In practice, there are a large number of STFs and DFs due to the size of scans, therefore it is important to filter them. First, the pooling operator is used to reduce duplicates within a radius. Second, pooled STFs and DFs within some distance of LTFs are removed to eliminate false positives caused by localization drift. Finally, points inside visually observed regions of the map are removed.

C. Map-free LiDAR Scan Classification

The classification method defined in III-B is limited by the necessity of static map information \mathcal{M} . Therefore, this work uses supervised learning to train a model to reproduce classifications for $\{p_i^j\}_{j=1:n_i}$ in scan s_i . Similarly to the ground-truth, non-map points are filtered by pooling and then by removing those in previously inspected regions.

1) *Dataset and Data Acquisition*: The collected dataset \mathcal{D} consists of tuples of data from the ground truth classification model. The tuples are given as $\mathcal{D} = \{(x_i, s_i, s_i^{\text{class}})\}_{i=1}^N$, where x_i represents robot pose, s_i is the raw LiDAR scan data, and s_i^{class} is the classified scan. N is the total number of data points collected. Collecting a dataset using a real robot requires a human expert to control the robot over long periods of time. This approach is difficult to scale due to mechanical limits of the robot and difficulty of control over large, potentially out-of-sight places. To ease data acquisition we design a steerable cart platform (see fig. 3) to mimic the robot. Human operators easily maneuver this cart to generate the dataset without strain

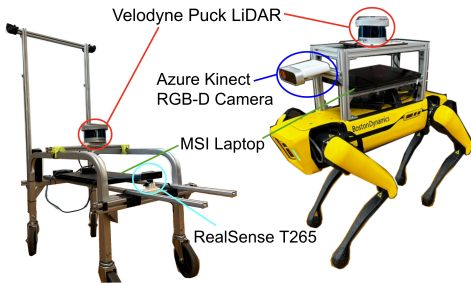


Fig. 3. A figure depicting the cart used for labeled data acquisition and the Spot robot used for deployment of the proposed method. The RealSense provides odometry estimate to the cart platform, required for localization and ground-truth estimation. The spot is equipped with an RGB-D Azure Kinect for detection during the search task.

to the robot. We mount a Velodyne Puck LiDAR for recording scan information and a front-mounted Intel RealSense T265 stereo camera to obtain the cart’s odometry estimate, required for running the ground-truth classification. Finally, a laptop is used to maintain the pose estimate [9], collecting the data and generating online ground-truth labels for the dataset. This laptop records 1) robot pose at each timestep, 2) raw scan data, and 3) classified scan from the ground-truth module for dataset \mathcal{D} . The Puck has $n_i = 897$ and classified scans are recorded at 5Hz. A dataset of size $N \simeq 145,000$ is collected in this study, representing roughly 8 hours of time. In practice, the model only receives raw scan data, pose estimate and previously predicted labels from the robot during operation and must classify pixel-wise the scan online.

2) *Architecture and Training*: We formulate pixel-wise LiDAR classification as a supervised learning problem during training and an auto-regressive problem during inference. Given dataset \mathcal{D} , we shuffle and batch the dataset between time steps and locations to minimize location-based and temporal bias during training. Because no map information is provided explicitly, we provide the model with a history buffer of k time steps for scan ranges and robot poses, and $k - 1$ previously estimated ground truth labels. Because we do not have access to ground truth labels at inference time, we corrupt the ground truth labels during training by randomly bit-flipping the classification of 10% of the labels, chosen by sampling indices from a uniform random distribution. We then take the exponential weighted average of the last $k - 1$ corrupted pixel-wise classifications to estimate the current pixel-wise classification. This estimate is concatenated with the $k - 1$ corrupted ground truth labels to produce a k -length matrix of estimated scan labels. During inference, the label history buffer is populated by previous estimates from the policy, cropped by a length k sliding-window. The history buffer is then concatenated with the updated pixel-wise exponential weighted average. At the initialization of inference, the policy is bootstrapped with zero-value poses, scans, and labels, and run for k steps of inference until the history buffer is initialized.

The policy consists of a temporal-convolutional encoder (TCN) for each input. Each encoder contains a single convolutional layer with scan-wise circular padding and a single linear layer. The scan and label encoders have kernel

size $[k, k]$, and the pose encoder has kernel size $[1, 3]$. Hyperbolic tangent activations are used for all layers. The output of each encoder is the same size as the LiDAR scan to be classified. The output of the pose encoder is summed with the output of the scan encoder as a pose correction, and then normalized by applying a hyperbolic tangent function. The resulting LiDAR scan encoding is multiplied element-wise with the label encoding. A threshold is applied to the raw logits such that each pixel is classified as either a map point or a non-map point. The policy is trained with mean squared error loss against ground truth classifications. Training for 20 epochs on a workstation Nvidia 3080 12Gb takes 3 minutes. The full model architecture is shown in Fig. 2.

D. Map Updates

Two global occupancy maps (search maps) are maintained. The first is a LiDAR global search map and the second is a visual global search map. Global search maps are implemented in this work using ROS Costmap2D [2]. All cells in both global maps are initialized to be unknown, $e = -1 \forall e \in \mathcal{E}$. The robot is equipped with a visual sensor with a cone shaped FoV, implemented as a triangular costmap. The LiDAR sensor has a 360 degree FoV, represented as a square-type costmap. Observations for both sensors are a set of range estimates to the nearest occupied point $e \in \mathcal{E}^{\text{occ}}$. Points between the robot and the nearest occupied point along each ray of the LiDAR scan are free points $e \in \mathcal{E}^{\text{free}}$. Given incoming observations from the robot, each global costmap is updated as free space $e = 0$ or occupied $e = 1$. This process is shown in Fig. 1(d).

E. Multisensor Frontier Exploration

The planning module seeks to generate a viewpoint at each planning step that results in the highest likelihood to find the target of interest. This is achieved in several steps: candidate viewpoints are generated, viewpoints are scored, and finally the point with the highest score is fed to the robot for navigation to that point.

1) *Candidate Viewpoint Generation*: Frontier points in each of the two global search maps are generated using a process similar to [33], shown in Fig. 1(e). Any free cell ($e = 0$) adjacent to an unknown cell ($e = -1$) is a frontier edge, which are grouped together into frontiers. Candidate viewpoints at frontiers are similar to those of [32]. First, a set of vision based viewpoints are generated by clustering frontiers on the visual global search map. Next, a set of LiDAR based viewpoints are generated by clustering frontiers on the LiDAR global search map. Each frontier cluster becomes four candidate viewpoints, facing each direction, to account for the limited FoV of the vision sensor.

2) *Viewpoint Selection*: Candidate viewpoints are selected based on a computationally efficient heuristic utility function. High value viewpoints are those that are 1) near the robot, 2) allow inspection of many unknown map points and 3) result in inspection of non-map points. This process is shown in Fig. 1(f). The utility functions is a weighted sum of the following:

- Subtract path distance from robot position to the viewpoint
- Add a reward for expected number of unknown cells discovered at that viewpoint
- Add a reward for viewpoints with frontiers near the path to the candidate viewpoint
- Add a reward for viewpoints that result in inspection of a scaled number non-map points

Scaling parameters on each term are tuned during experiments. Weights are set such that the agent is inclined to prioritize non-map points and those viewpoints that result in high number of expected cells discovered. The next waypoint is selected by sending the highest utility viewpoint, x_{next}^* , to the robot.

IV. RESULTS

We test three hypotheses through our evaluation: (1) The proposed approach to inform an exploring agent with non-map features is effective at finding search targets, (2) LIVES reduces detection time compared against existing exploration algorithms, and (3) The proposed method can be deployed on real robot hardware and used in a human environment.

A. LiDAR Scan Classification

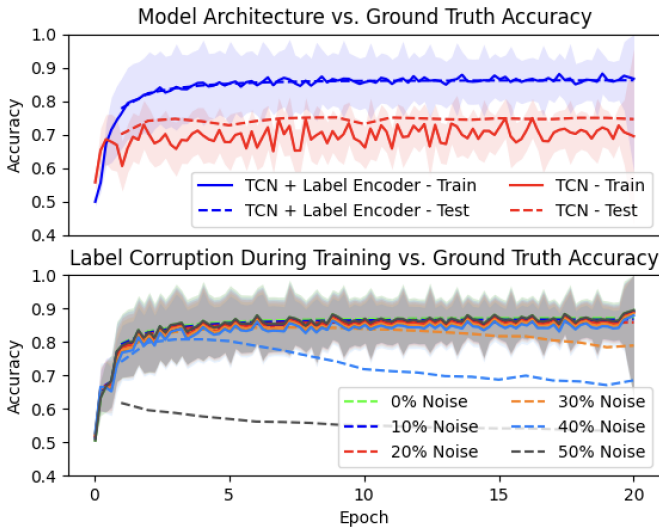


Fig. 4. Ablation studies over policy architecture (top) and injected noise during training (bottom). The inclusion of the label history buffer yields 11.63% higher test accuracy. The policy is robust up to 30% to bit-flipping errors in the label history buffer. The mean accuracy depicts the 5-step moving average.

First we compare the learned classification policy to the ground truth classifier. The output of the policy is a vector of size n_i normalized between -1 and 1 for each scan point. If this value is non-negative, the point is classified as a member of \mathcal{E}^{map} . Otherwise the point is classified as a member of $\mathcal{E}^{\text{non-map}}$. We express performance in terms of per-scan accuracy of the classified LiDAR scans from the neural network estimator versus ground truth scan classification from map information. This metric for a classified scan s_i^{class} at time i compared to ground truth $s_i^{\text{class, true}}$ is given by

$$\text{accuracy} = \frac{1}{n_i} \sum_{j=0}^{n_i} \{+1 \text{ if } p_i^j == p_i^{j, \text{true}} \text{ else } 0\} \quad (4)$$

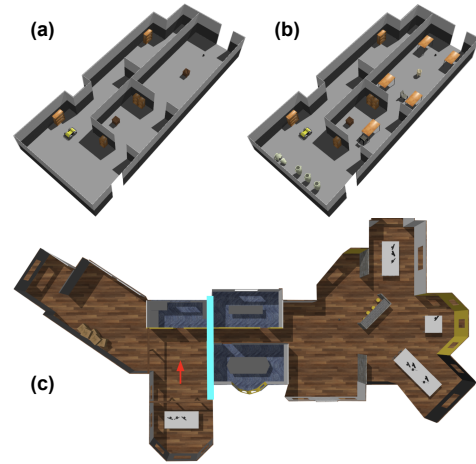


Fig. 5. The Apartment simulation environment (top row) in the Easy configuration (a) and Hard Configuration (b). The Office (c) shows the robot starting position as a red arrow. Easy setup involves the search target to the left of the cyan line and Hard involves the search target on the right of the cyan line.

The final test accuracy of the policy compared to ground truth is $86.19\% \pm 0.03\%$ with no a priori map requirement. We perform two ablation studies, modulating the model architecture and injected noise during training, with results in Fig. 4. The inclusion of the label encoder is responsible for a 11.63% increase in test accuracy. Because the robot moves relatively slowly compared to the policy update frequency, recently predicted labels strongly bias the current estimate toward the correct classification. We fix the history buffer to 9 time steps, corresponding to 1.8 seconds. The history buffer enables the policy to reason about its environment even though no reference map is provided. During training, uniform random noise is injected into the label history buffer to simulate inference-time auto-regressive accumulated errors. The policy is robust up to 30% of injected noise before the policy begins to over-fit and performance degrades. We select a policy trained with 10% injected noise to deploy on the robot. All ablation studies were performed with a fixed seed (0) and initialized with identical weights. We do not tune the random seed.

B. Simulation and Baseline Comparison

Simulations are performed using Gazebo-ROS on the Turtlebot [4]. ROS move base is used for navigation [1]. Baselines are: 1) a lightly modified version of [32] (Multi-sensor Frontier Exploration), 2) the Next-Best View Planner (NBVP) [7], 3) a Rapidly-Exploring Random Tree (RRT) [3], and 4) LIVES given ground-truth scan classifications. The Multisensor baseline is equivalent to LIVES and ground-truth without contextual LiDAR information. Two Gazebo world environments are tested with easy and hard setups in each. The first map is the apartment (20x30m) and examines the impact of non-target objects on LIVES (see Fig. 5(a-b)). Here the easy setting incorporates fewer objects in the environment and the search target being closer to the robot while hard is defined by more objects in the environment and larger distance to the target. The second map is the office (25x45m) and tests the method in a large environment under

Map Name	Target Difficulty	NBVP [7]	RRT [3]	Multisensor Frontier Exploration [32]	Ground Truth Classification	LIVES (Our Method)
Apartment	Easy	112(70%)	72(80%)	36 (100%)	34(100%)	34(100%)
	Hard	177(30%)	128(60%)	106 (100%)	92(100%)	90(100%)
Office	Easy	70(80%)	54 ± (80%)	34 (100%)	26(100%)	24(100%)
	Hard	300(0%)	111 (80%)	141(90%)	99(100%)	105(100%)

TABLE I
AVERAGE TIME (S) FOR EACH METHOD TO FIND THE OBJECT OF INTEREST IN THE GIVEN SIMULATION ENVIRONMENT.

significantly varied target position (see Fig. 5(c)). The easy and hard settings are defined by the search target being in the same or different half of the environment as the robot starting position. Both difficulty levels in each map are repeated 10 times. Average detection times and success rates are reported in Table I. The time limit given to planners is 2 and 3 minutes in the apartment easy and hard settings then 3 and 5 minutes in the office easy and hard settings. Trials where the planner fails or the time limit is reached are reported as a failure and failed trials are reported as the maximum allotted time.

Results indicate that LIVES, the Ground-Truth variant and the Multisensor Frontier Exploration method significantly outperform the RRT and NBVP baselines in all settings except for the hard office setting, where the RRT method performs similarly to LIVES and Ground-Truth methods. In the easy apartment setting we observe similar performance among the three planners. However in the hard setting, where LIVES and Ground-Truth perform nearly identically, there is roughly a 15% improvement with the addition of the knowledge of non-map points compared with the Multisensor method. We see a large gap, however, in the easy office setting with a near 30% improvement with the addition of contextual LiDAR information over the Multisensor variant. In the hard office setting, LIVES and Ground-Truth variant outperform the RRT method by 5-12%. Overall, the results indicate that the proposed method to inform the frontier planner with non-map information outperforms the baselines across the full spectrum of environments. We hypothesize this is due to the requirement for the exploration planners to exhaustively explore the environment, whereas the proposed method focuses on non-map points, allowing the agent to move on when the target is unlikely to be nearby. These results support hypotheses (1) and (2) that contextual LiDAR information significantly improves performance in the search task.

C. Hardware Experiments

Experiments are in a 20mx30m indoor apartment setting. The environment is out of distribution as it is not included in dataset \mathcal{D} used to train the pixel-wise classification policy. The platform used is a Boston Dynamics Spot robot with a Velodyne Puck LiDAR and Azure Kinect RGB-D camera. The search target of interest is a small rolling suitcase and YOLOv5 [16] is used for detection of the object. On detection, the exploration node is shut down and the task is complete. We perform several trials over varying initial robot position and target locations. A time lapse of one experiment is shown in Fig. 6 where the search target is situated behind the robot starting position. This example demonstrates the benefit of non-map information. In (b), if selecting simply based on number of un-

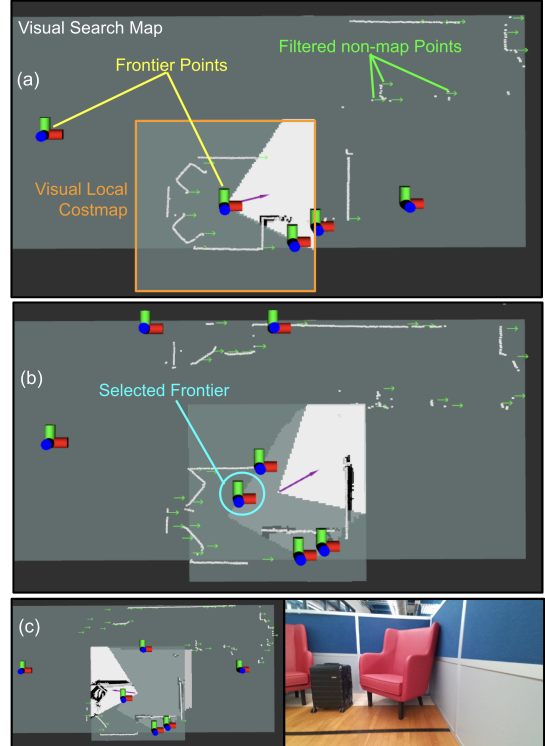


Fig. 6. A time lapse of one experiment scenario. In (a) the robot pose is a purple arrow with the visual costmap, global search map, frontier points and non-map points shown. The raw scan data is shown as small white squares. The target object is behind the robot starting position. Figure (b) occurs immediately before a planning step, wherein the marked frontier is selected due to the high occurrence of non-map points nearby. (c) occurs after the planning step and results in detection.

known cells discovered, the agent may select another frontier, for example the one on the left hand side. However, equipped with this contextual information the agent selects the frontier that enables inspection of many non-map features nearby. The success of LIVES onboard a real robot verify hypothesis (3). Videos of experiments can be found on the project website <https://sites.google.com/view/lives-icra-2024/home>.

V. CONCLUSIONS

We present a method for visual search in unseen environments using contextual LiDAR information to inform planning. Results show LIVES to outperform the closest of several baseline methods in varied environments by 10-30%. Ablative studies on the map-free scan classifier are performed to validate the choice in architecture and training scheme. Furthermore, the proposed approach is deployed on a real robot in an unseen environment. Experiments certify both the visual search planner and the learning method for map-free scan classification in real-world scenarios. Ongoing work aims to extend the LIVES planner to multiple robots.

REFERENCES

- [1] URL <https://github.com/ros-planning/navigation>.
- [2] URL http://wiki.ros.org/costmap_2d.
- [3] URL https://github.com/hasauino/rrt_exploration.
- [4] URL <https://www.turtlebot.com/turtlebot3/>.
- [5] Stefan Andreas Baur, David Josef Emmerichs, Frank Moosmann, Peter Pinggera, Björn Ommer, and Andreas Geiger. Slim: Self-supervised lidar scene flow and motion segmentation. In *Proceedings of the IEEE/CVF International Conference on Computer Vision*, pages 13126–13136, 2021.
- [6] Graeme Best, Rohit Garg, John Keller, Geoffrey A Hollinger, and Sebastian Scherer. Resilient multi-sensor exploration of multifarious environments with a team of aerial robots. In *Robotics: Science and Systems (RSS)*, 2022.
- [7] Andreas Bircher, Mina Kamel, Kostas Alexis, Helen Oleynikova, and Roland Siegwart. Receding horizon “next-best-view” planner for 3d exploration. In *2016 IEEE International Conference on Robotics and Automation (ICRA)*, pages 1462–1468. IEEE, 2016.
- [8] Joydeep Biswas and Manuela Veloso. Depth camera based indoor mobile robot localization and navigation. In *2012 IEEE International Conference on Robotics and Automation*, pages 1697–1702. IEEE, 2012.
- [9] Joydeep Biswas and Manuela M Veloso. Episodic non-markov localization. *Robotics and Autonomous Systems*, 87:162–176, 2017.
- [10] Jeffrey A Caley, Nicholas RJ Lawrance, and Geoffrey A Hollinger. Deep learning of structured environments for robot search. *Autonomous Robots*, 43:1695–1714, 2019.
- [11] Yuhong Cao, Tianxiang Hou, Yizhuo Wang, Xian Yi, and Guillaume Sartoretti. Ariadne: A reinforcement learning approach using attention-based deep networks for exploration. *arXiv preprint arXiv:2301.11575*, 2023.
- [12] Benjamin Charrow, Sikang Liu, Vijay Kumar, and Nathan Michael. Information-theoretic mapping using cauchy-schwarz quadratic mutual information. In *2015 IEEE International Conference on Robotics and Automation (ICRA)*, pages 4791–4798. IEEE, 2015.
- [13] Xieyuanli Chen, Benedikt Mersch, Lucas Nunes, Rodrigo Marcuzzi, Ignacio Vizzo, Jens Behley, and Cyrill Stachniss. Automatic labeling to generate training data for online lidar-based moving object segmentation. *IEEE Robotics and Automation Letters*, 7(3):6107–6114, 2022.
- [14] Anna Dai, Sotiris Papatheodorou, Nils Funk, Dimos Tzoumanikas, and Stefan Leutenegger. Fast frontier-based information-driven autonomous exploration with an mav. In *2020 IEEE international conference on robotics and automation (ICRA)*, pages 9570–9576. IEEE, 2020.
- [15] Alok Jhaldiyal and Navendu Chaudhary. Semantic segmentation of 3d lidar data using deep learning: a review of projection-based methods. *Applied Intelligence*, 53(6):6844–6855, 2023.
- [16] Glenn Jocher. YOLOv5 by Ultralytics, May 2020. URL <https://github.com/ultralytics/yolov5>.
- [17] Brian J Julian, Sertac Karaman, and Daniela Rus. On mutual information-based control of range sensing robots for mapping applications. *The International Journal of Robotics Research*, 33(10):1375–1392, 2014.
- [18] Minghua Liu, Yin Zhou, Charles R Qi, Boqing Gong, Hao Su, and Dragomir Anguelov. Less: Label-efficient semantic segmentation for lidar point clouds. In *European Conference on Computer Vision*, pages 70–89. Springer, 2022.
- [19] Max Lodel, Bruno Brito, Alvaro Serra-Gómez, Laura Ferranti, Robert Babuška, and Javier Alonso-Mora. Where to look next: Learning viewpoint recommendations for informative trajectory planning. In *2022 International Conference on Robotics and Automation (ICRA)*, pages 4466–4472. IEEE, 2022.
- [20] Benedikt Mersch, Xieyuanli Chen, Ignacio Vizzo, Lucas Nunes, Jens Behley, and Cyrill Stachniss. Receding moving object segmentation in 3d lidar data using sparse 4d convolutions. *IEEE Robotics and Automation Letters*, 7(3):7503–7510, 2022.
- [21] François Pomerleau, Francis Colas, Roland Siegwart, and Stéphane Magnenat. Comparing icp variants on real-world data sets: Open-source library and experimental protocol. *Autonomous robots*, 34:133–148, 2013.
- [22] Charles R Qi, Hao Su, Kaichun Mo, and Leonidas J Guibas. Pointnet: Deep learning on point sets for 3d classification and segmentation. In *Proceedings of the IEEE conference on computer vision and pattern recognition*, pages 652–660, 2017.
- [23] Charles Ruizhongtai Qi, Li Yi, Hao Su, and Leonidas J Guibas. Pointnet++: Deep hierarchical feature learning on point sets in a metric space. *Advances in neural information processing systems*, 30, 2017.
- [24] Santhosh K Ramakrishnan, Ziad Al-Halah, and Kristen Grauman. Occupancy anticipation for efficient exploration and navigation. In *Computer Vision—ECCV 2020: 16th European Conference, Glasgow, UK, August 23–28, 2020, Proceedings, Part V 16*, pages 400–418. Springer, 2020.
- [25] Manish Saroya, Graeme Best, and Geoffrey A Hollinger. Online exploration of tunnel networks leveraging topological cnn-based world predictions. In *2020 IEEE/RSJ International Conference on Intelligent Robots and Systems (IROS)*, pages 6038–6045. IEEE, 2020.
- [26] Tixiao Shan and Brendan Englot. Lego-loam: Lightweight and ground-optimized lidar odometry and mapping on variable terrain. In *2018 IEEE/RSJ International Conference on Intelligent Robots and Systems (IROS)*, pages 4758–4765. IEEE, 2018.
- [27] Chee Sheng Tan, Rosmiwati Mohd-Mokhtar, and Mohd Rizal Arshad. A comprehensive review of coverage path planning in robotics using classical and heuristic algorithms. *IEEE Access*, 2021.
- [28] Yuezhan Tao, Yuwei Wu, Beiming Li, Fernando Cladera,

- Alex Zhou, Dinesh Thakur, and Vijay Kumar. Seer: Safe efficient exploration for aerial robots using learning to predict information gain. In *2023 IEEE International Conference on Robotics and Automation (ICRA)*, pages 1235–1241. IEEE, 2023.
- [29] Hugues Thomas, Charles R Qi, Jean-Emmanuel Deschaud, Beatriz Marcotegui, François Goulette, and Leonidas J Guibas. Kpconv: Flexible and deformable convolution for point clouds. In *Proceedings of the IEEE/CVF international conference on computer vision*, pages 6411–6420, 2019.
- [30] Hugues Thomas, Ben Agro, Mona Gridseth, Jian Zhang, and Timothy D Barfoot. Self-supervised learning of lidar segmentation for autonomous indoor navigation. In *2021 IEEE International Conference on Robotics and Automation (ICRA)*, pages 14047–14053. IEEE, 2021.
- [31] Hugues Thomas, Matthieu Gallet de Saint Aurin, Jian Zhang, and Timothy D Barfoot. Learning spatiotemporal occupancy grid maps for lifelong navigation in dynamic scenes. In *2022 International Conference on Robotics and Automation (ICRA)*, pages 484–490. IEEE, 2022.
- [32] Eduard Vidal, Narcís Palomeras, Klemen Istenič, Nuno Gracias, and Marc Carreras. Multisensor online 3d view planning for autonomous underwater exploration. *Journal of Field Robotics*, 37(6):1123–1147, 2020.
- [33] Brian Yamauchi. A frontier-based approach for autonomous exploration. In *Proceedings 1997 IEEE International Symposium on Computational Intelligence in Robotics and Automation CIRA'97. Towards New Computational Principles for Robotics and Automation'*, pages 146–151. IEEE, 1997.
- [34] Maciej Zamorski, Maciej Zieba, Piotr Klukowski, Rafal Nowak, Karol Kurach, Wojciech Stokowiec, and Tomasz Trzcinski. Adversarial autoencoders for compact representations of 3d point clouds. *Computer Vision and Image Understanding*, 193:102921, 2020.
- [35] Kaiyu Zheng, Anirudha Paul, and Stefanie Tellex. A system for generalized 3d multi-object search. *arXiv preprint arXiv:2303.03178*, 2023.
- [36] Yuke Zhu. *Closing the Perception-action Loop: Towards General-purpose Robot Autonomy*. Stanford University, 2019.